processes

MDPI

Article

Temperature Distribution Estimation in a Dwight–Lloyd Sinter Machine Based on the Combustion Rate of Charcoal Quasi-Particles

Ziming Wang [1,*], Ko-ichiro Ohno [2,*], Shunsuke Nonaka [3], Takayuki Maeda [2] and Kazuya Kunitomo [2]

1 Department of Materials Process Engineering, Kyushu University, 744 Motooka, Nishi-ku, Fukuoka 819-0395, Japan
2 Department of Materials Science and Engineering, Faculty of Engineering, Kyushu University, 744 Motooka, Nishi-ku, Fukuoka 819-0395, Japan; maeda@zaiko.kyushu-u.ac.jp (T.M.); kunitomo@zaiko.kyushu-u.ac.jp (K.K.)
3 Department of Materials Process Engineering, Graduate School of Engineering, Kyushu University, Now at JFE Steel, 1 Mizushima-kawasaki-dori, Kurashiki, Okayama Prefecture 712-8511, Japan; sh-nonaka@jfe-steel.co.jp
* Correspondence: ou.shimei.515@s.kyushu-u.ac.jp (Z.W.); ohno.ko-ichiro.084@m.kyushu-u.ac.jp (K.-i.O.)

Received: 27 February 2020; Accepted: 25 March 2020; Published: 31 March 2020

Abstract: The coke combustion rate in an iron ore sintering process is one of the most important determining factors of quality and productivity. Biomass carbon material is considered to be a coke substitute with a lower CO_2 emission in the sintering process. The purpose of this study was to investigate the combustion rate of a biomass carbon material and to use a sintering simulation model to calculate its temperature profile. The samples were prepared using alumina powder and woody biomass powder. To simplify the experimental conditions, alumina powder, which cannot be reduced, was prepared as a substitute of iron ore. Combustion experiments were carried out in the open at 1073 K~1523 K. The results show that the combustion rates of the biomass carbon material were higher than that of coke. The results were analyzed using an unreacted core model with one reaction interface. The kinetic analysis found that the k_c of charcoal was higher than that of coke. It is believed that the larger surface area of charcoal may affect its combustion rate. The analysis of the sintering simulation results shows that the high temperature range of charcoal was smaller than that of coke because of charcoal's low fixed carbon content and density.

Keywords: coke combustion rate; charcoal combustion rate; iron ore sintering process; temperature distribution; biomass; quasi-particle

1. Introduction

CO_2 emission from Japan's industrial sector is much higher than that from other sectors. In 2017, it accounted for approximately 37.2% of the total emission. In the industrial sector, the iron and steel-making industry accounts for approximately 39.4% of energy consumption. The steel industry emits approximately 13% of the CO_2 in Japan [1]. The demands of global environmental conservation require a greenhouse gas reduction. Currently, approximately 80 million tons of pig iron are produced by blast furnace annually in Japan. Coal and coke are used as reducing materials and heat sources, respectively, and a large amount of CO_2 is emitted in the iron-making process. Therefore, the development of innovative technologies is required to reduce the CO_2 emission.

Trees absorb carbon dioxide during photosynthesis. When wood from forests is burned as fuel, carbon dioxide is generated. If the forest is renewed after tree cutting, the carbon dioxide will be

absorbed by the trees again during the growth process. Thus, the use of wood for energy is carbon neutral. Therefore, using wood instead of fossil fuels makes it possible to reduce carbon dioxide emissions and contribute to the prevention of global warming [2].

It is increasingly difficult to prepare a sintering iron ore due to the high price of raw materials, environmental regulations and inferior quality raw materials. Limited work [3–6] has been conducted to investigate the application of biomass in the sintering process to replace coke breeze, with this work mainly focused on its environmental impacts and low substitution rates. Therefore, it is necessary to improve the sintering iron ore method. In the sintering process, the coke combustion rate is one of the most important determining factors of quality and productivity.

However, little research has been conducted on the combustion behavior of biomass carbon material quasi-particles during the sintering process. The purpose of this study was to investigate the combustion rate of a biomass carbon material and use a sintering simulation model to calculate its temperature profile.

2. Experimental Sample and Procedure

To simulate the test particles, the samples were prepared using alumina powder and woody biomass powder. The woody biomass powder used in this study was commercial mangrove charcoal, which is normally used for barbecues. To simplify the experimental conditions, alumina powder was prepared as a substitute for iron ore. Alumina eliminated the effects of melt formation, reduction and re-oxidation of iron ore during coke combustion. Charcoal powder with a particle diameter of −125 μm and 125~250 μm was used in this experiment. The particle size of iron ore was to simulate the adhere powder layer, but not the coke particle. Coke powder with the same particle diameter was used to compare the results. Alumina powder with a particle diameter of −250 μm was prepared to match the particle size of the iron ore. The analysis of the results of prepared carbon material are listed in Table 1. Compared with coke, charcoal has a lower ash ratio and higher volatile matter content and therefore charcoal has a lower fixed carbon. The surface area of charcoal is higher than that of coke. This was also observed by an SEM, as shown in Figure 1. Figure 2 shows the overall view of raw materials and samples. After the alumina and coke powders were mixed, 0.5 mass % flour was mixed as a binder. The flour was just used to enable keeping the tablet shape until it was inserted to the platinum basket. It was thought that the effect of the flour could be negligible, because flour evaporates at a lower temperature—600 K—than the experimental temperature in this study. Then, the mixture was pressed into 10 mm diameter tablets by stainless dies. The height of the tablet was 10 mm with a void ratio of 35%. The void ratio was decided from the information on the tablet volume and the true density of the sample mixture. Each true density of the sample materials was measured by pycnometer. The weight ratio of coke in each sample was fixed at 20 mass %. To ensure that the volume ratio of the samples was the same as the hematite and alumina samples, 22.1 mass % coke with 77.9 mass % alumina and 20.8 mass % charcoal with 79.2 mass % alumina was also prepared.

Table 1. Properties of carbon materials.

	Ash (mass %)	V.M. (mass %)	Fix.C. (mass %)	Specific Surface Area (m^2/g)
Charcoal (−125 μm)	1.84	29.2	69.0	61.0
Charcoal (125~250 μm)				28.5
Coke (−125 μm)	10.1	1.71	88.2	2.59
Coke (125~250 μm)				0.92

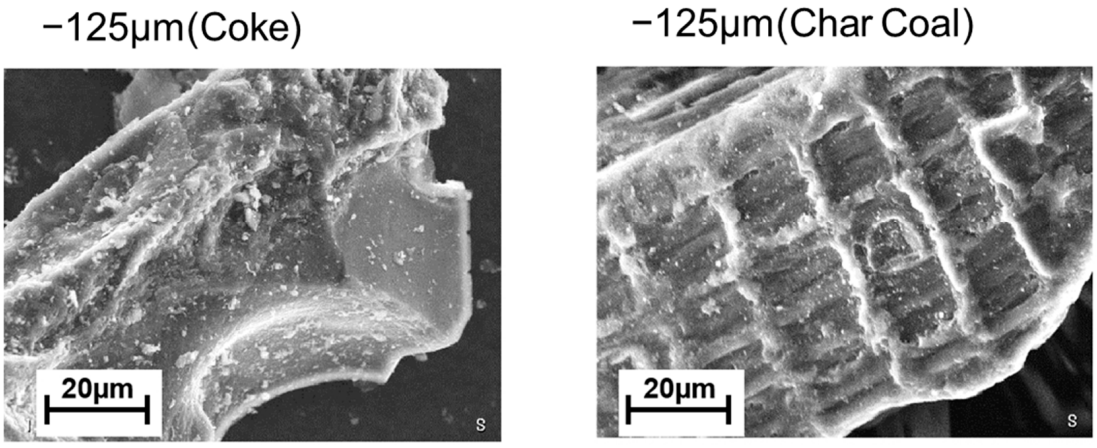

Figure 1. Scanning electron micrograph of coke and charcoal (−125 μm).

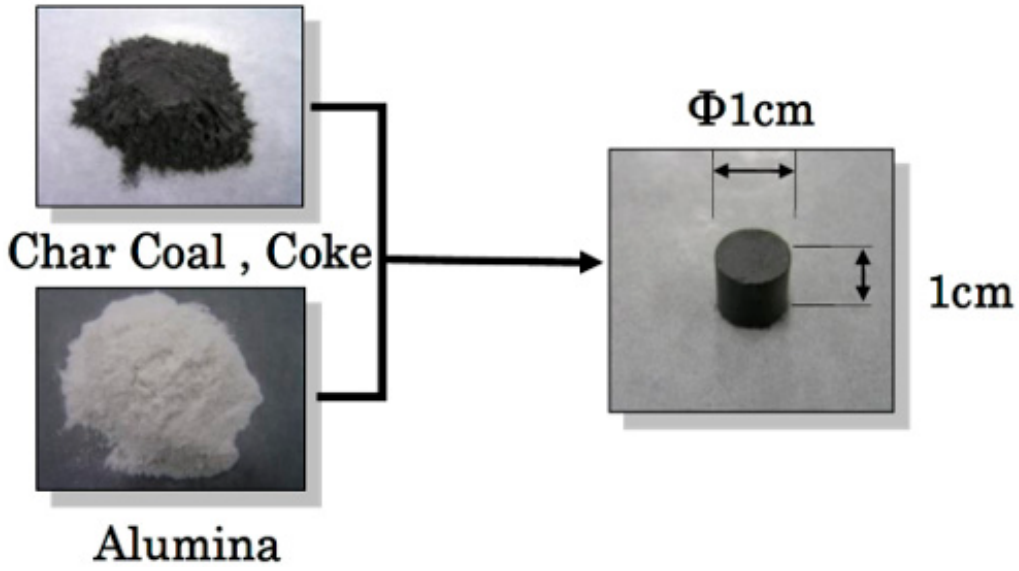

Figure 2. Overall view of the raw materials and the sample.

The measurement of the sample weight loss during coke combustion was done by the thermobalance shown in Figure 3. The sample was placed in a platinum basket. A vertical electric resistance furnace was used to do isothermal heating. The isothermal zone was heated up to 1073 K, 1223 K, 1373 K and 1523 K. Before the combustion experiment, heat treatment of the samples was carried out at each of the given temperatures in a N_2 atmosphere for 30 mins to remove water, Volatile matter (V.M.) and the binder from the samples. Then, air was passed through the reaction tube. The air flow rate was 4 NL/min. When a weight change in the sample was not observed, the experiment was terminated. It was hypothesized that coke ash did not influence the weight loss of the sample because the amount of coke in every sample stayed the same.

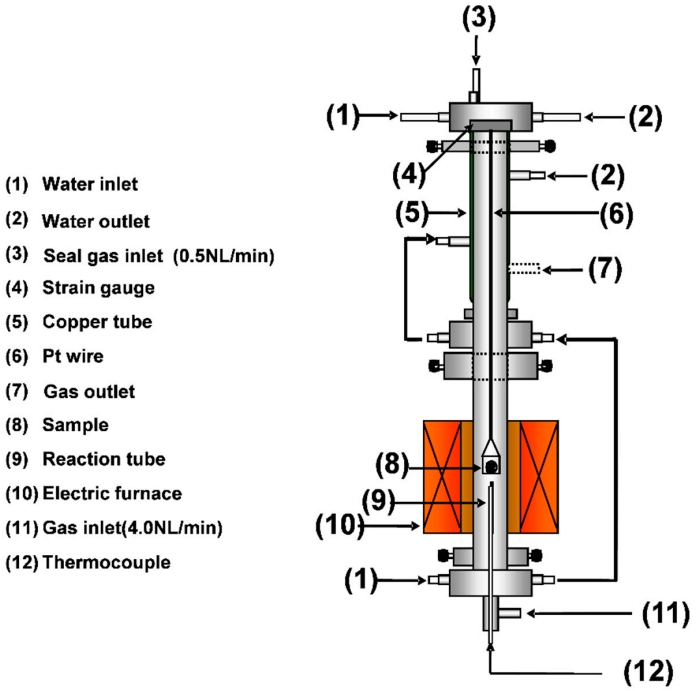

Figure 3. Schematic of the device used in the experiment.

3. Results

The reaction ratio in the study was defined as the removal ratio of fixed carbon from the sample. A carbon combustion reaction can be described using the following chemical reaction, if CO gas formation is ignored:

$$C(s) + O_2(g) = CO_2(g) \quad (1)$$

In the combustion experiment, the sample weight loss was attributed to the decrease in the amount of fixed carbon. Therefore, the reaction ratio (F) at a reaction time can be described by Equation (2):

$$F = \frac{\Delta w_t}{W} \quad (2)$$

Fractional reaction curves at 1073 K are shown in Figure 4. The figure shows that combustion rates of charcoal were quicker than those of coke. This tendency was also observed at 1223 K, 1373 K and 1523 K.

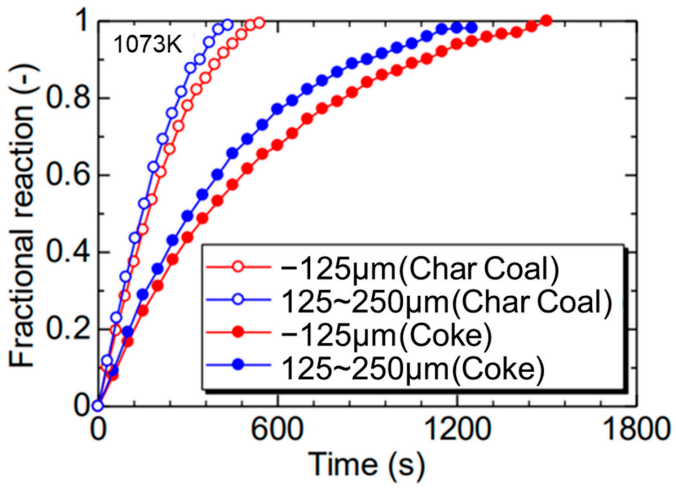

Figure 4. Fractional reaction curves of coke and charcoal combustion at 1073 K.

To verify the reaction mechanism of the combustion reaction, samples with a reaction ratio of 50% were also prepared under 1073 K and 1523 K and cross-sectional and microscopic observations were made. Figures 5 and 6 show the cross-sectional observation and the microstructure at the reaction interfaces of each sample. It was clear that the combustion reaction was a topochemical reaction.

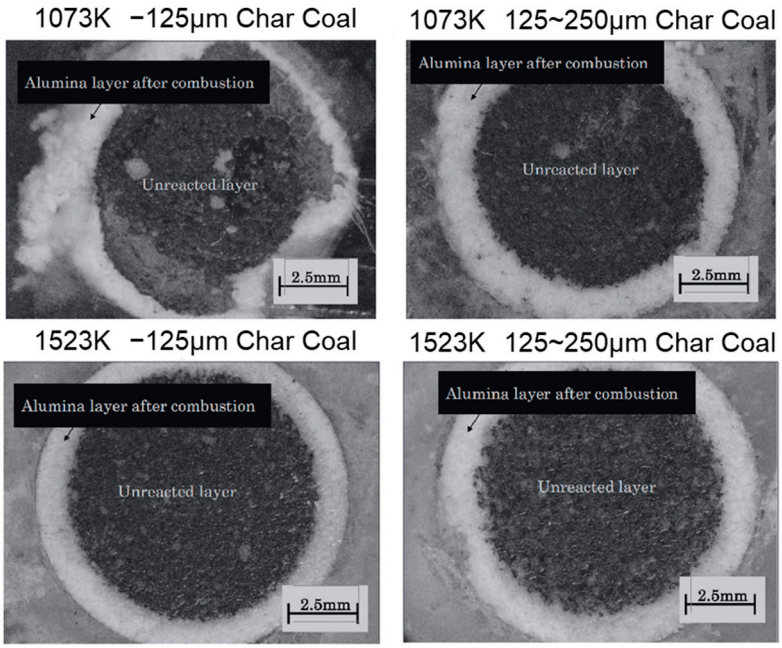

Figure 5. Cross-sectional view of the samples.

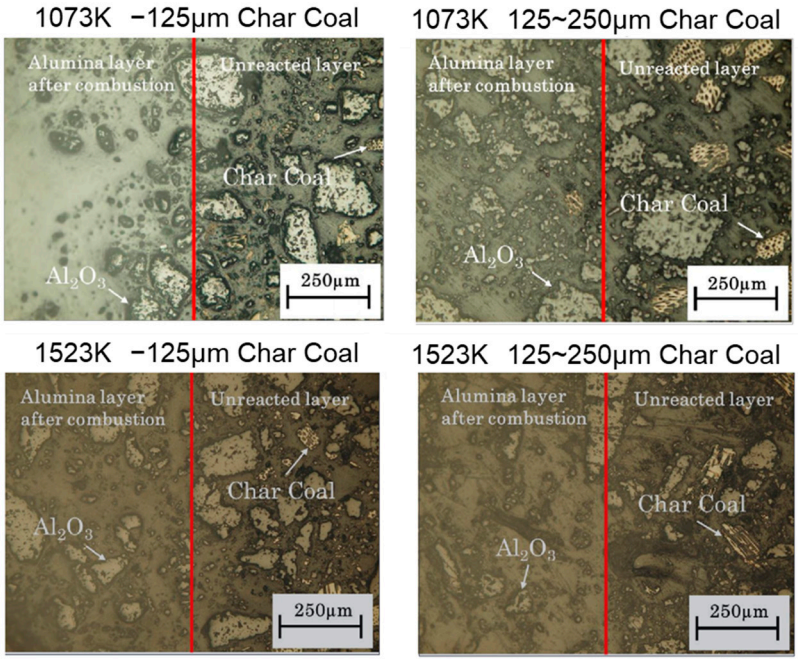

Figure 6. Microstructure of the samples at the reaction interface.

4. Kinetic Analysis

4.1. Unreacted Core Model for Coke

From the fractional reaction curves obtained from the combustion experiment, the combustion reaction rate constant was determined using the unreacted core model [7]. The combustion reaction has five processes [8].

1. O_2 transport from the gas phase to the particle surface through the gas film:

$$-\dot{n}_{g\cdot O_2} = 4\pi r_0^2 k_f \left(C_{O_2} - C_{O_2\cdot s}\right) \tag{3}$$

2. O_2 transport from the particle surface to the reaction interface through the alumina powder layer after coke combustion:

$$-\dot{n}_{d\cdot O_2} = (D_{O_2})_{eff} \frac{4\pi r_0 r_i}{r_0 - r_i} \left(C_{O_2\cdot s} - C_{O_2\cdot i}\right) \tag{4}$$

3. The combustion reaction at the reaction interface:

$$-\dot{R} = 4\pi r_i^2 k_c \left(C_{O_2\cdot i} - \frac{C_{CO_2\cdot i}}{K}\right) \tag{5}$$

4. CO_2 transport from the reaction interface to the particle surface through the alumina powder layer after coke combustion:

$$\dot{n}_{d\cdot CO_2} = (D_{CO_2})_{eff} \frac{4\pi r_0 r_i}{r_0 - r_i} \left(C_{CO_2\cdot i} - C_{CO_2\cdot s}\right) \tag{6}$$

5. CO_2 transport from the particle surface to the gas phase through the gas film:

$$\dot{n}_{g\cdot CO_2} = 4\pi r_0^2 k_f \left(C_{CO_2\cdot s} - C_{CO_2}\right) \tag{7}$$

The overall rate equation can be described by the quasi-steady state analysis method below:

$$-\dot{n} = \frac{4\pi r_0^2 \left(\frac{K}{1+K}\right)\left(C_{O_2} - C_{CO_2}\right)}{\frac{1}{k_f} + \frac{1}{D_e}\cdot\frac{r_0(r_o - r_i)}{r_i} + \frac{1}{k_c}\cdot\frac{K}{1+K}\left(\frac{r_0}{r_i}\right)^2} \tag{8}$$

$$\frac{1}{D_e} = \frac{K}{1+K}\left(\frac{1}{(D_{O_2})_{eff}} + \frac{1}{K(D_{CO_2})_{eff}}\right) \tag{9}$$

Equation (8) can be expressed by the following equation, assuming that the combustion reaction of coke was an irreversible reaction and the equilibrium constant K infinite:

$$-\dot{n} = \frac{4\pi r_0^2 C_{O_2}}{\frac{1}{k_f} + \frac{1}{D_e}\cdot\frac{r_0(r_0 - r_i)}{r_i} + \frac{1}{k_c}\cdot\left(\frac{r_0}{r_i}\right)^2} \tag{10}$$

$\dot{n}$ can be replaced by the following equation:

$$-\dot{n} = -\frac{d}{dt}\left(\frac{4}{3}\pi r_i^3 \rho_{Cm}\right) = -4\pi r_i^2 \rho_{Cm}\cdot\frac{dr_i}{dt} \tag{11}$$

The reaction ratio F is expressed by Equation (12):

$$F = 1 - \left(\frac{r_i}{r_0}\right)^3 \tag{12}$$

When Equations (10)–(12) are combined and integrated under boundary conditions; $r = r_0$ at $t = 0$ and $r = r_i$ at $t = t$, Equation(13) is obtained:

$$t = \frac{\rho_{Cm} r_0}{C_{O_2}}\cdot\left[\frac{F}{3k_f} + \frac{d_r}{16D_e}\left\{3 - 3(1-F)^{\frac{2}{3}} + 2F\right\} + \frac{1}{k_C}\left\{1 - (1-F)^{\frac{1}{3}}\right\}\right] \tag{13}$$

The gas film mass transfer coefficient, k_f, can be calculated from Ranz–Marshall's Equation [9]. The value of the effective diffusion coefficient in the alumina layer, D_e, and the interfacial reaction rate coefficient of coke, k_C, was obtained by parameter-fitting using the nonlinear least-squares method to the fractional reaction curves.

D_e, and k_C can be expressed by substituting the coefficients in Arrhenius' equation as shown:

$$k_C = A_{(k_C)} exp\left(-\frac{E_{a(k_C)}}{RT}\right) \tag{14}$$

$$D_e = A_{(D_e)} exp\left(-\frac{E_{a(D_e)}}{RT}\right) \tag{15}$$

Equations (13) and (14) can be transformed into the following equations:

$$lnk_C = -\frac{E_{a(k_C)}}{R} \cdot \frac{1}{T} + lnA_{(k_C)} \tag{16}$$

$$lnD_e = -\frac{E_{a(D_e)}}{R} \cdot \frac{1}{T} + lnA_{(D_e)} \tag{17}$$

Figure 7 shows the Arrhenius plot of k_c. The values of k_c are at the same level in all samples. The temperature dependence of k_c is expressed as

Coke	(−125 μm)	$k_c = 6.02 \times 10^{-2} \exp(-9.32 \times 10^3/RT)$	(m/s)
	(125~250 μm)	$k_c = 4.51 \times 10^{-2} \exp(-5.12 \times 10^3/RT)$	(m/s)

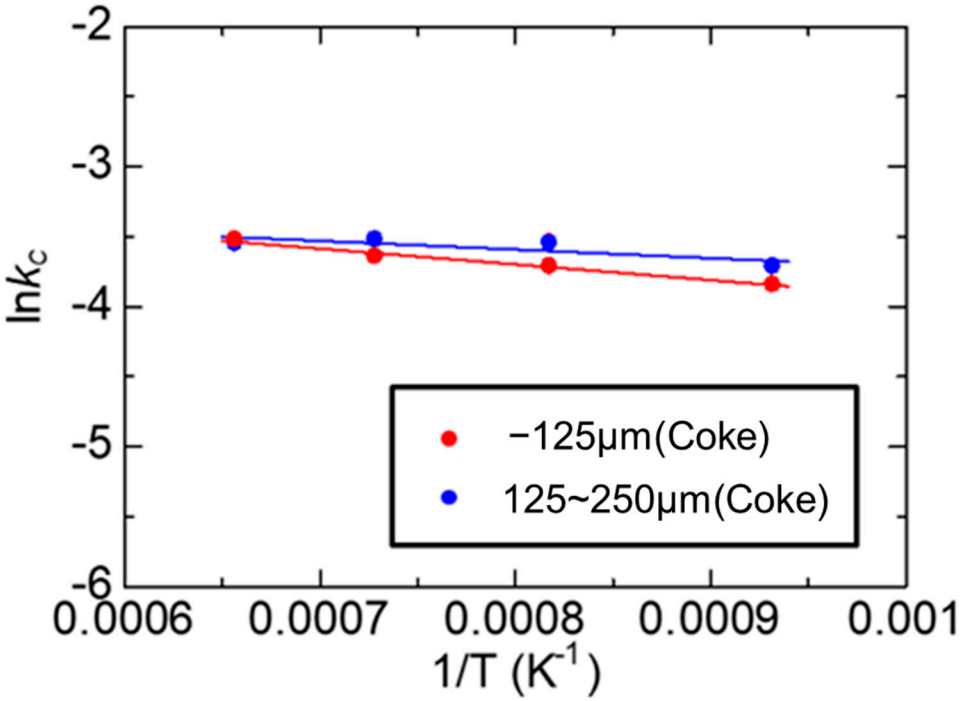

Figure 7. Temperature dependence of the reaction rate constants k_c.

Figure 8 shows the Arrhenius plot of D_e. The temperature dependence of D_e can be expressed as

Coke	(−125 μm)	$D_e = 1.79 \times 10^{-3} \exp(-36.4 \times 10^3/RT)$	(m/s)
	(125~250 μm)	$D_e = 3.06 \times 10^{-3} \exp(-36.6 \times 10^3/RT)$	(m/s)

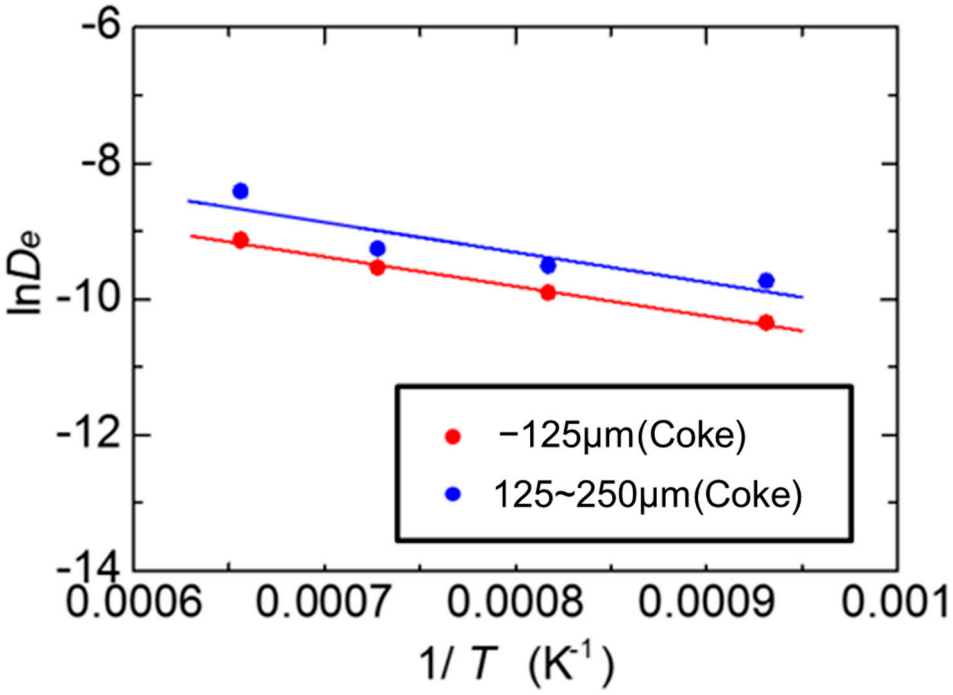

Figure 8. Temperature dependence of the effective diffusivities D_e.

4.2. Chemical Reaction Control Step for Charcoal

Because the surface area of charcoal is larger than that of coke, when a combustion reaction takes place, the reaction area of charcoal will also be larger. Moreover, due to the low ash ratio in the charcoal, the O_2 transportation rate in the alumina layer will be large. Therefore, the reaction is based on the chemical reaction control step.

For the charcoal samples, the chemical reaction control step can be used in the analysis method shown below:

The combustion reaction at the reaction interface can be expressed by Equation (5).

The combustion rate can be expressed as

$$-\dot{n} = \frac{4\pi r_0^2 \left(\frac{K}{1+K}\right)\left(C_{O_2} - \frac{C_{CO_2}}{K}\right)}{\frac{1}{k_c} \cdot \frac{K}{1+K}\left(\frac{r_0}{r_i}\right)^2} \tag{18}$$

Under boundary conditions, $r = r_0$ at $t = 0$ and $r = r_i$ at $t = t$, and this gives Equation (19):

$$\left[1 - (1-F)^{\frac{1}{3}}\right] = \frac{C_{O_2}}{\rho c_m r_0} k_c t \tag{19}$$

Based on the reaction curves obtained by the experiments, k_c was determined using the unreacted core model [3].

k_C can be substituted in Arrhenius' equation as shown by Equation (14) which also can be transformed as Equation (16).

Figure 9 shows the Arrhenius plot of k_c.

The temperature dependence of k_c can be expressed as

Coke	(−125 μm)	$kc = 8.24 \times 10^{-3} \exp\left(-10.6 \times 10^3 / RT\right)$	(m/s)
	(125~250 μm)	$kc = 8.54 \times 10^{-3} \exp\left(-10.3 \times 10^3 / RT\right)$	(m/s)

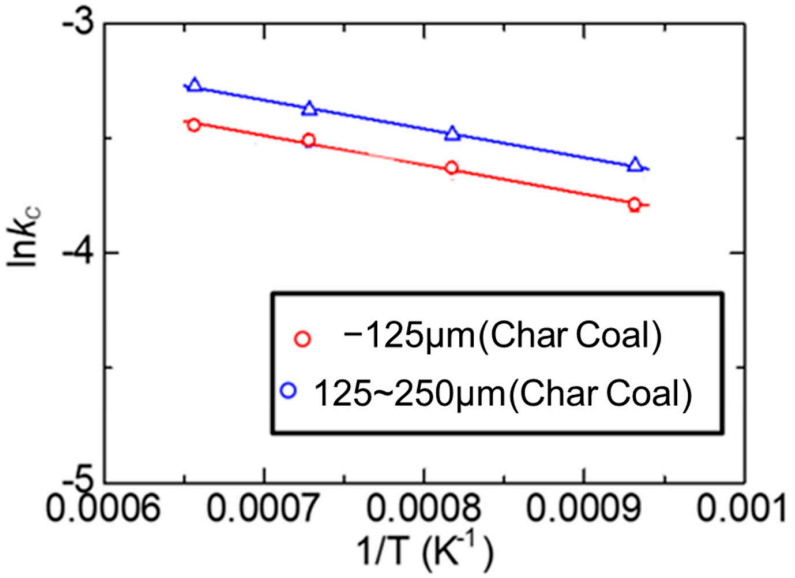

Figure 9. Temperature dependence of the reaction rate constants k_c.

5. Sintering Simulation Model

5.1. Simulation Method

The simulation condition was based on the study results using Ohno's model [10]. The model has S'-type, C-type and P-type quasi-particles as shown in Figure 10. The S' type was calculated using Hottel's equation [11–13], while the C and P types were calculated based the results obtained in this study.

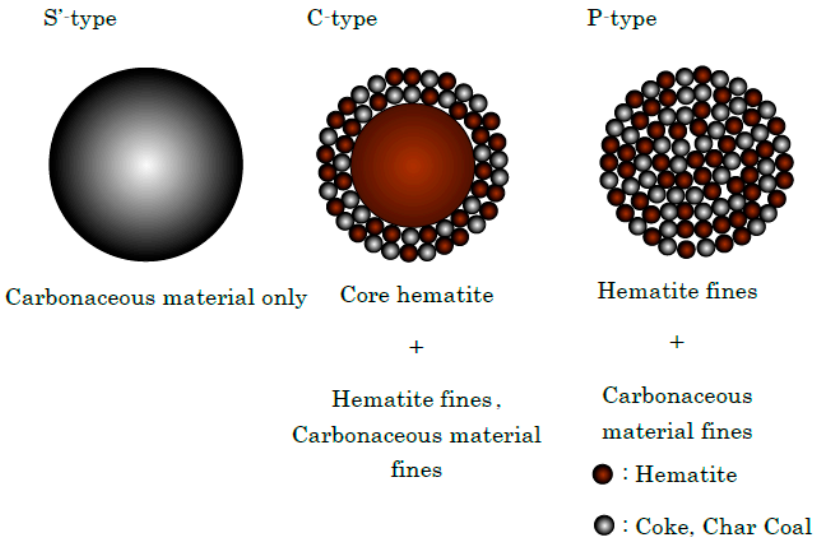

Figure 10. Classification of the quasi-particles.

Our mathematical model is based on the Dwight–Lloyd sinter machine and the calculation range is from the ignition point on the pallet to the discharge of the sinter ore.

The numerical analysis was based on the control volume method shown in Figure 11. The control volume method is obtained by dividing the analysis target region into equal minute portions. Various basic equations, representing phenomena, such as the continuous and energy conservation equations, govern the inside of the analysis target area and are relational equations to be established in each control volume. Assuming that these control volumes are in a sufficiently small area, there would not

be a large error even if the changes in various quantities inside the control volumes were linear or approximated to be constant values. In other words, changes in various quantities in a certain control volume can be represented using values at a representative point in the control volume adjacent to the representative point. In our mathematical model, the sintering material layer was divided into minute control volumes in one dimension, the basic governing equations were discretized, and each difference approximation equation was solved using an explicit method.

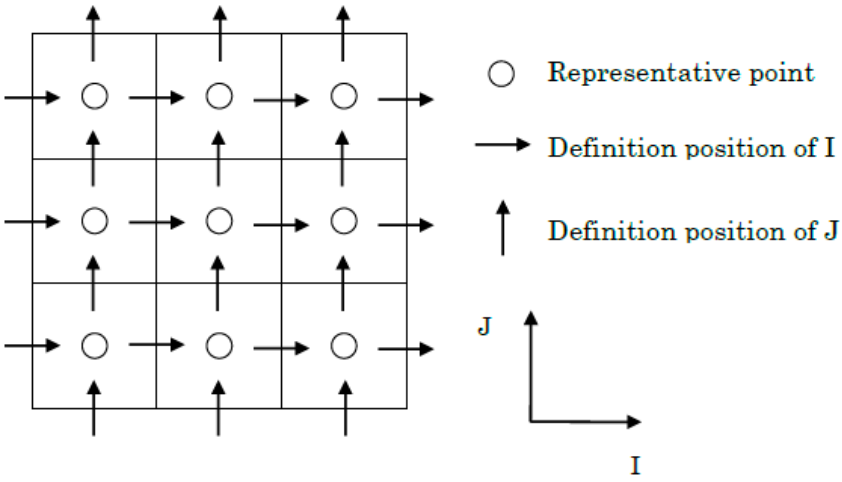

Figure 11. Pattern diagram of the control volume.

In the model used, the temperature distribution was estimated considering the combustion of carbonaceous materials, the decomposition reaction of $CaCO_3$, the evaporation and condensation of water, and the formation and solidification of calcium ferrite melt according to Ohno's model [10].

D_e depends on coke distribution.

The combustion reaction rate of the quasi-particles is expressed by Equations (20) and (21):

$$r^*_{Quasi-particle} = 4\pi r^2_{Quasi-particle} k' C_{O_2} \tag{20}$$

$$k' = 1/\left(\frac{1}{k_f} + \frac{r_0(r_0 - r_i)}{D_e r_i} + \frac{r_0^2}{k_c r_i^2}\right) \tag{21}$$

In this equation, D_e has a value of 10^8 because the resistance of the diffusion can be ignored.

The material balance is calculated using Equation (22):

$$\frac{\rho_{i\cdot x}\big|_{t+\Delta t} - \rho_{i\cdot x}\big|_t}{\Delta t} = -\frac{(\rho_{Z+\Delta Z} u_i)\big|_{Z+\Delta Z} - (\rho_Z u_{i-1})\big|_Z}{\Delta Z} + r^*_{i,x} \tag{22}$$

The material balance equations of N_2, O_2, CO_2 and H_2 respectively, can be expressed as follows:

$$\frac{\partial\left(\rho_{N_2} u\right)}{\partial Z} = -\frac{\partial \rho_{N_2}}{\partial t} \tag{23}$$

$$\frac{\partial\left(\rho_{O_2} u\right)}{\partial Z} = -\frac{\partial \rho_{O_2}}{\partial t} - r^*_{Coke} \tag{24}$$

$$\frac{\partial\left(\rho_{CO_2} u\right)}{\partial Z} = -\frac{\partial \rho_{CO_2}}{\partial t} + r^*_{Coke} + r^*_{CaCO_3} \tag{25}$$

$$\frac{\partial\left(\rho_{H_2O} u\right)}{\partial Z} = -\frac{\partial \rho_{H_2O}}{\partial t} + r^*_{H_2O} \tag{26}$$

Because convection did not occur in the solid phase, the thermal budget of the phase considering heat transfer and reaction heat can be represented as

$$\rho_s C_{P\cdot s}\frac{\partial T_s}{\partial t} - \frac{6(1-\varepsilon_a)}{\dot{d}}h\left(T_g - T_s\right) + H_{Coke}\left(r^*_{Coke}n_{Coke} + r^*_{Quasi-paritcle}n_{Quasi-particle}\right) + H_{CaCO_3}r^*_{CaCO_3}n_{CaCO_3} + H_{H_2O\cdot V}r^*_{H_2O\cdot V} + H_{CF\cdot G}r^*_{CF\cdot G} + H_{CF\cdot S}r^*_{CF\cdot S} = k\frac{\partial^2 T_s}{\partial Z^2} \quad (27)$$

The thermal budget of the gas phase factoring the heat transfer and combustion reaction heat can be expressed as

$$\rho_g C_{P\cdot g}\frac{\partial T_g}{\partial t} - \frac{6(1-\varepsilon_a)}{\dot{d}}h\left(T_s - T_g\right) + C_{P\cdot g}\frac{\partial \rho_g u T_g}{\partial Z} = k\frac{\partial^2 T_g}{\partial Z^2} \quad (28)$$

The particles were charged in the control volume. Therefore, the pressure loss of the fluid also needed to be considered. The pressure loss of a laminar-turbulent transition area can be represented by Ergun's equation as shown:

$$\frac{\Delta P}{\Delta Z} = \frac{150(1-\varepsilon_a)^2}{(\varphi d)^2 {\varepsilon_a}^3}\cdot\frac{\mu_g}{\rho_g}U + 1.75\frac{1-\varepsilon_a}{\varphi d {\varepsilon_a}^3}U^2 \quad (29)$$

5.2. Calculation Conditions

Table 2 lists the common calculation conditions for the sintering process. The composition of raw materials was set to simplify the calculation condition. The influence of MgO was not considered in this study. The particle size of hematite was set to 2.5 mm and 0.25 mm. It was assumed that 2.5 mm and 0.25 mm were the sizes of the nuclear particle and the adhering fine ores, respectively, in the quasi-particle. The 5.1 mass % charcoal calculation was compared with the 4 mass % coke calculation when the fixed carbon content is the same which means that the combustion heat of coke and charcoal during this process is the same. However, in this study, the effect of V.M. was not discussed. As a thought, the gas generated when V.M. is heated may improve the permeability and affect the temperature profile in the same way as a gas fuel injection, mentioned by Oyama [14]. Further research is needed to clarify this factor.

Table 2. Common calculation conditions.

▪ Sinter Bed	
Bed depth	450 mm
Porosity of sinter bed	35%
▪ Composition of Raw materials	
Hematite	85.0 mass %
Lime (CaO)	10.0 mass %
Moisture	5.0 mass %
Coke, Charcoal	4.0 mass % (additionally)
Charcoal	5.1 mass % (additionally)
▪ Diameter of Raw Materials	
Hematite	2.5 mm:0.25 mm ≈ 88.6:11.4
Lime (CaO)	2.0 mm
▪ Others	
Initial temperature	298 K
Ignition temperature	1573 K
Ignition time	90 s
Gas flow rate (outlet)	0.6 m/s
Calculation cell	5 mm
Time step	0.001 s
Courant number	0.2

Table 3 lists the state of the coke quasi-particles in the sinter bed for calculation using the date of the sinter pot test based on Hida's study [15].

Table 3. Existing state of the coke quasi-particles in the sinter bed.

Existing State of Coke (%)			Total	Amount of Coke and Charcoal in Sinter Bed (%)
S'-Type	C-Type	P-Type		
40.0	30.0	30.0	100	4.0, 5.1

5.3. Calculation Results

Figures 12 and 13 show the temperature profiles of the cases of coke and charcoal at a depth of 20 cm and 40 cm, respectively. The basic case was 4 mass% coke mixing condition. It was compared with cases of 4 mass % and 5.1 mass % charcoal mixing conditions. The influence of particle size is not apparent. Compared with the results for coke, charcoal has a lower temperature profile and a shorter holding time at a high temperature. This is thought to be due to the low fixed carbon content and the density of charcoal which leads to the presence of unreacted charcoal. As a result, the temperature of charcoal in all the sinter cakes was lower than that of coke.

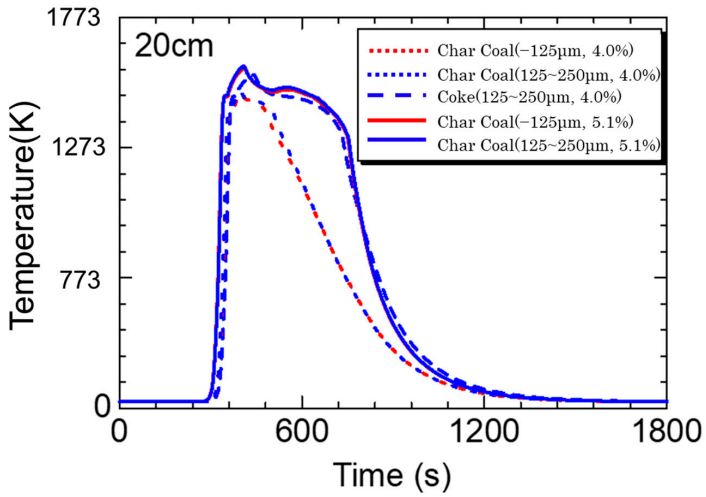

Figure 12. Calculation results of the temperature profile (20cm).

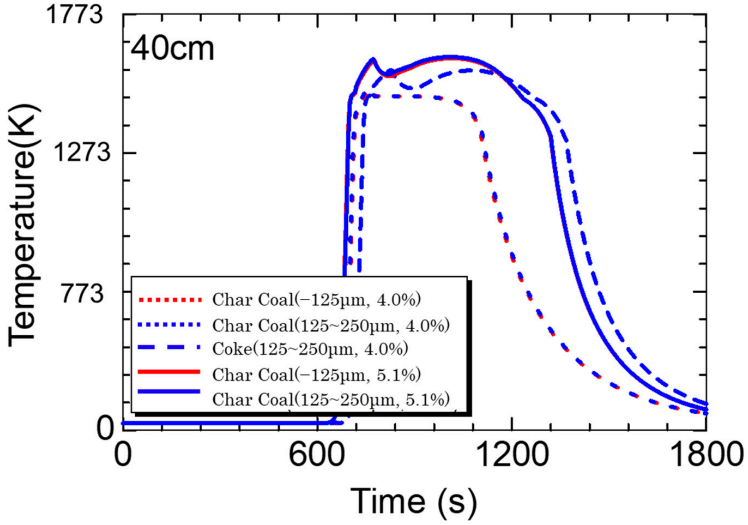

Figure 13. Calculation results of the temperature profile (40cm).

However, when the amount of charcoal was 5.1 mass %, the holding times at a high temperature of both kinds of carbon material were at the same level. The highest temperature of charcoal was higher than that of coke. The rate of the temperature increase of charcoal was also faster than that of coke. This is because the combustion rate of charcoal is higher than that of coke, i.e., if the fixed carbon content of charcoal is equivalent to that of coke, the temperature profile of the same level can be obtained. Therefore, the sintering simulation results of this study show that there are probabilities that charcoal can replace coke in the sintering process.

6. Conclusions

The study aimed to understand the combustion rate of a biomass carbon material using a sintering model to calculate its temperature profile. The following conclusions were made:

- Compared with coke, the reaction curves of charcoal combustion show that the combustion reaction of charcoal is faster.
- The interfacial chemical reaction rate coefficient of charcoal for the experimental data was calculated as follows:

Coke	(−125 μm)	$kc = 8.24 \times 10^{-3} \exp\left(-10.6 \times 10^3 / RT\right)$	(m/s)
	(125~250 μm)	$kc = 8.54 \times 10^{-3} \exp\left(-10.3 \times 10^3 / RT\right)$	(m/s)

- Calculations using the rate equation obtained in the sintering simulation model found that the high temperature range of charcoal is smaller than that of coke due to charcoal's low fixed carbon content and density.
- If the fixed carbon content of charcoal is the same as that of coke, which means that the combustion heat of carbon materials is the same, a temperature profile of the same level can be obtained.
- The sintering simulation results suggest that there are probabilities that biomass carbon materials can replace coke in the sintering process.

Author Contributions: Conceptualization, K.-i.O., and K.K.; Methodology, T.M.; Validation, K.-i.O., T.M., and Z.W.; Formal Analysis, S.N., and T.M.; Investigation, S.N.; Data Curation, Z.W., S.N., and T.M.; Writing-Original Draft Preparation, Z.W., and S.N.; Writing-Review and Editing, K.-i.O., and T.M.; Visualization, Z.W., and S.N.; Supervision, K.K.; Project Administration, K.-i.O. All authors have read and agreed to the published version of the manuscript.

Funding: This research received no external funding.

Conflicts of Interest: The authors declare no conflict of interest.

Nomenclature

$A_{(kc,De)}$	Frequency factor (m/s)
$C_{(O2,\,CO2)}$	O_2 or CO_2 concentration in the gas phase (mol/m^3)
$C_{(O2,\,CO2)\cdot i}$	O_2 or CO_2 concentration at the reaction interface (mol/m^3)
$C_{(O2,\,CO2)\cdot s}$	O_2 or CO_2 concentration at the particle surface (mol/m^3)
C_p	Specific heat (J/kg/K)
d	Particle size (m)
D_e	Effective diffusion coefficient in the Al_2O_3 powder layer (m^2/s)
$(D_{O2,\,CO2})_{eff}$	Effective diffusion coefficient of O_2 or CO_2 in the Al_2O_3 powder layer (m^2/s)
$E_{a(kc,De)}$	Activation energy (J/mol)
F	Reaction ratio (–)
H	Reaction heat of each reaction (J/mol)
h	Convection heat transfer coefficient (J/m^2/s/K)
K	Equilibrium constant (–)

k_C	Interfacial chemical reaction rate coefficient (m/s)
k_f	Mass transfer coefficient in the gas film (m/s)
k	Heat conductivity (J/m/s/K)
k'	Overall reaction rate (m/s)
$n_{(\text{Coke, Quasi-particle, Lime, Ore})}$	The amount of coke, quasi-particle, lime and ore among unit volume (-)
ΔP	Pressure loss (atm)
r_0	Initial radius (m)
r_i	Radius of the non-reaction nucleus (m)
$r_{i,x}$ *	Generation rate of the component x in the number i cell (kg/s/m^3)
$r_{Quasi\text{-}particle}$	Distance from the left of the particle to the reaction interface of the quasi-particle (m)
r *	Reaction ratio of the component in the sample (–)
r *$_{Quasi\text{-}particle}$	Reaction rate per one particle of the quasi-particle (mol/s)
T_g	Temperature of gas in the control volume (K)
T_s	Temperature of solid in the control volume (K)
Δw_t	Sample weight change (kg)
U	Superficial velocity (m/s)
u	Gas flow rate (m/s)
W	Weight change of the sample during the experiment (kg)
ΔZ	Length of the control volume (m)
P_x	Density of component x (kg/m^3)
ρ_{Cm}	Carbon concentration in the sample (mol/m^3)
$\rho_{N2,\ O2,CO2,\ H2O}$	Density of gas in the sample(kg/m^3)
ε_a	Porosity (-)
Φ	(Surface area of a ball which has the same volume with the particle)/(Surface area of the particle) (-)
μ_g	Viscosity of gas (Pa·s)

References

1. *Japan's National Greenhouse Gas Emissions in Fiscal Year 2017 (Final Figures)*; Ministry of the Environment: Tokyo, Japan, 2019.
2. Takeshima, S. Biomass, Carbon-neutral and Renewable Energy. K. *J. JIME* **2012**, *47*, 133. [CrossRef]
3. Lovel, R.R.; Vining, K.R.; Dell'Amico, M. The influence of fuel reactivity on iron ore sintering. *ISIJ Int.* **2009**, *49*, 195–202. [CrossRef]
4. Zandi, M.; Martinez-Pacheco, M.; Fray, T. Biomass for iron ore sintering. *Miner. Eng.* **2010**, *23*, 1139–1145. [CrossRef]
5. Ooi, T.; Aries, E.; Ewan, B.; Thompson, D.; Anderson, D.R.; Fisher, R.; Fray, T.; Tognarelli, D. The study of sunflower seed husks as a fuel in the iron ore sintering process. *Miner. Eng.* **2008**, *21*, 167–177. [CrossRef]
6. Gan, M.; Fan, X.; Chen, X.; Ji, Z.; Lv, W.; Wang, Y.; Yu, Z.; Jiang, T. Reduction of pollutant emission in iron ore sintering process by applying biomass fuels. *ISIJ Int.* **2012**, *52*, 1574–1578. [CrossRef]
7. Yagi, T.; Ono, Y. A method of analysis for reduction of iron oxide in mixed-control kinetics. *Trans. ISIJ* **1968**, *8*, 377.
8. Ohno, K.; Noda, K.; Nisioka, K.; Maeda, T.; Shimizu, M. Combustion rate of coke in quasi-particle at iron ore sintering process. *ISIJ Int.* **2013**, *53*, 1588–1593. [CrossRef]
9. Ranz, W.E.; Marshall, W.R. Evaporation from drops. *Chem. Eng. Prog.* **1952**, *48*, 173–180.
10. Ohno, K.; Noda, K.; Nisioka, K.; Maeda, T.; Shimizu, M. Effect of coke combustion rate equation on numerical simulation of temperature distribution in iron ore sintering process. *ISIJ Int.* **2013**, *53*, 1642–1647. [CrossRef]
11. Tu, C.M.; Davis, H.; Hottel, H.C. Combustion rate of carbon-combustion of spheres in flowing gas streams. *Ind. Eng. Chem.* **1934**, *26*, 749–757. [CrossRef]
12. Davis, H.; Hottel, H.C. Combustion rate of carbon-combustion at a surface overlaid with stagnant gas. *Ind. Eng. Chem.* **1934**, *26*, 889–892. [CrossRef]
13. Parker, A.S.; Hottel, H.C. Combustion rate of carbon study of gas-film structure by microsampling. *Ind. Eng. Chem.* **1936**, *28*, 1334–1341. [CrossRef]

14. Oyama, N.; Iwami, Y.; Yamamoto, T.; Machida, S.; Higuchi, T.; Sato, H.; Sato, M.; Takeda, K.; Watanabe, Y.; Shimizu, M.; et al. Development of secondary-fuel injection technology for energy reduction in the iron ore sintering process. *ISIJ Int.* **2011**, *51*, 913–921. [CrossRef]
15. Hida, Y.; Sasaki, M.; Enokido, T.; Umezu, Y.; Iida, T.; Uno, S. Effect of the existing state of coke breeze in quasi-particles of raw mix on coke combustion in the sintering process. *Tetsu-to-Hagané* **1982**, *68*, 400–409. [CrossRef]

© 2020 by the authors. Licensee MDPI, Basel, Switzerland. This article is an open access article distributed under the terms and conditions of the Creative Commons Attribution (CC BY) license (http://creativecommons.org/licenses/by/4.0/).